Journal of Advanced Research 43 (2023) 205–218

Contents lists available at ScienceDirect

Journal of Advanced Research

journal homepage: www.elsevier.com/locate/jare

Original Article

GPX4 deficiency-dependent phospholipid peroxidation drives motor deficits of ALS

Long-Fang Tu [a,b,c,g], Tian-Ze Zhang [a,b,c], Yang-Fan Zhou [a,b,c], Qing-Qing Zhou [a,b,c], Hai-Biao Gong [a,b,c], Lei Liang [a,b,c,d,*], Lin-Na Hai [a,b,c], Nan-Xin You [a,b,c], Yang Su [e], Yong-Jun Chen [e], Xu-Kai Mo [f], Chang-Zheng Shi [f], Liang-Ping Luo [f], Wan-Yang Sun [a,b,c], Wen-Jun Duan [a,b,c,d,*], Hiroshi Kurihara [a,b,c], Yi-Fang Li [a,b,c,*], Rong-Rong He [a,b,c,d,*]

[a] Guangdong Engineering Research Center of Chinese Medicine & Disease Susceptibility, Jinan University, Guangzhou 510632, China
[b] International Cooperative Laboratory of Traditional Chinese Medicine Modernization and Innovative Drug Development of Chinese Ministry of Education (MOE), College of Pharmacy, Jinan University, Guangzhou 510632, China
[c] Guangdong Province Key Laboratory of Pharmacodynamic Constituents of TCM and New Drugs Research, College of Pharmacy, Jinan University, Guangzhou 510632, China
[d] School of Traditional Chinese Medicine, Jinan University, Guangzhou 510632, China
[e] South China Research Center for Acupuncture and Moxibustion, Medical College of Acu-Moxi and Rehabilitation, Guangzhou University of Chinese Medicine, Guangzhou 510006, China
[f] Medical Imaging Center, First Affiliated Hospital of Jinan University, Guangzhou 510632, China
[g] Computer-Aided Drug Discovery Research Center, Shenzhen Institutes of Advanced Technology, Chinese Academy of Sciences, Shenzhen 518055, China

HIGHLIGHTS

- The level of phospholipid peroxidation in spinal cord is increased in ALS mouse model.
- Anti-phospholipid peroxidation treatment reduces spinal motor neuron loss in ALS mice.
- The expressions of GPX4 are decreased in lumbar spinal cords of ALS mice and patients.
- Knockdown of Gpx4 results in loss of spinal motor neurons and abnormal neuromuscular connections.
- Intrathecal injection of *GPX4*-AAV to overexpress GPX4 alleviates the pathological phenomenon of ALS.

GRAPHICAL ABSTRACT

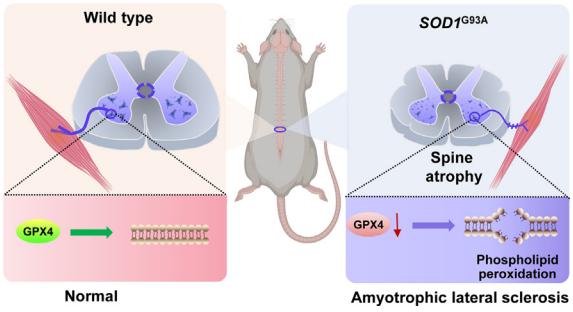

ARTICLE INFO

Article history:
Received 4 November 2021
Revised 15 January 2022
Accepted 27 February 2022
Available online 4 March 2022

Keywords:
ALS
Phospholipid peroxidation
GPX4

ABSTRACT

Amyotrophic lateral sclerosis (ALS) is a progressive neurodegenerative disease characterized by oxidative stress that triggers motor neurons loss in the brain and spinal cord. However, the mechanisms underlying the exact role of oxidative stress in ALS-associated neural degeneration are not definitively established. Oxidative stress-generated phospholipid peroxides are known to have extensive physiological and pathological consequences to tissues. Here, we discovered that the deficiency of glutathione peroxidase 4 (GPX4), an essential antioxidant peroxidase, led to the accumulation of phospholipid peroxides and resulted in a loss of motor neurons in spinal cords of ALS mice. Mutant human *SOD1*^{G93A} transgenic mice were intrathecally injected with neuron-targeted adeno-associated virus (AAV) expressing *GPX4* (*GPX4*-AAV) or phospholipid peroxidation inhibitor, ferrostatin-1. The results showed that impaired motor

Peer review under responsibility of Cairo University.
* Corresponding authors at: Guangdong Engineering Research Center of Chinese Medicine & Disease Susceptibility, Jinan University, Guangzhou 510632, China.
E-mail addresses: leiliang@jnu.edu.cn (L. Liang), duanwj@jnu.edu.cn (W.-J. Duan), liyifang706@jnu.edu.cn (Y.-F. Li), rongronghe@jnu.edu.cn (R.-R. He).

https://doi.org/10.1016/j.jare.2022.02.016
2090-1232/© 2022 The Authors. Published by Elsevier B.V. on behalf of Cairo University.
This is an open access article under the CC BY-NC-ND license (http://creativecommons.org/licenses/by-nc-nd/4.0/).

SOD1^{G93A} transgenic mice
Spinal cord

performance and neural loss induced by *SOD1*^{G93A} toxicity in the lumbar spine were substantially alleviated by ferrostatin-1 treatment and AAV-mediated *GPX4* delivery. In addition, the denervation of neuron-muscle junction and spinal atrophy in ALS mice were rescued by neural GPX4 overexpression, suggesting that GPX4 is essential for the motor neural maintenance and function. In comparison, conditional knockdown of *Gpx4* in the spinal cords of *Gpx4*$^{fl/fl}$ mice triggered an obvious increase of phospholipid peroxides and the occurrence of ALS-like motor phenotype. Altogether, our findings underscore the importance of GPX4 in maintaining phospholipid redox homeostasis in the spinal cord and presents GPX4 as an attractive therapeutic target for ALS treatment.
© 2022 The Authors. Published by Elsevier B.V. on behalf of Cairo University. This is an open access article under the CC BY-NC-ND license (http://creativecommons.org/licenses/by-nc-nd/4.0/).

Introduction

Amyotrophic lateral sclerosis (ALS) is a fatal neurodegenerative disease characterized by progressive degeneration of motor neuron in the brain and spinal cord [1–3]. Patients with ALS usually show muscle atrophy and gradually develop paralysis, eventually dying of respiratory muscle failure 3 to 5 years after being diagnosed [4]. Although ALS is a rare disease, the number of new cases continues to rise thereby imposing great socioeconomic burden on patients and their families [5–7]. Oxidative stress plays a central role in the onset and progression of ALS through the induction of neuronal excitotoxicity and astrocyte activation [8,9]. To date, due to undefined mechanism and the lack of specific therapeutic targets, there are still no effective disease-modifying therapies for ALS and current FDA-approved medications, such as edaravone and riluzole, only show modest effects on disease progression [10–12]. Hence, there is an urgent need to identify potential targets for ALS therapy.

In recent years, there is emerging evidence to support a correlation between accumulation of phospholipid peroxides and a variety of diseases including neurodegenerative diseases, cancer, etc [13–16]. Neuronal membrane phospholipids are rich in polyunsaturated fatty acid (PUFA) that are susceptible to peroxidative damage, ultimately leading to membrane structure modification and neuron death [17,18]. Hence, the peroxidation of phospholipids with PUFA has been regarded as an important parameter that reflects the degree of oxidative damage in neurons [19]. Given the importance of oxidative stress in ALS pathogenesis, further studies exploring the role of phospholipid peroxidation in ALS are warranted. Altered phospholipid metabolism and elevated level of 4-hydroxynonenal (4HNE), an end product of phospholipid peroxidation, have been revealed in the spinal cord of ALS mice and patients [20,21]. Accordingly, we speculate that phospholipid peroxidation-induced spinal cord damage might contribute to ALS disease progression.

A phospholipid peroxidation-associated cell death type, known as ferroptosis, is initiated by doubly- and triply-oxygenated arachidonic acid-containing phosphatidylethanolamines (PEs) [22]. Importantly, these highly active oxidized PEs can be reduced to less toxic hydroxy-PEs by an antioxidant enzymes glutathione peroxidase 4 (GPX4) [23]. This phospholipid-specific hydroperoxidase is essential for maintaining phospholipid redox balance, due to its unique ability to directly remove phospholipid peroxides in the presence of glutathione (GSH) [24,25]. Several studies have underscored the protective role of GPX4 in brain diseases, such as Alzheimer's disease, Parkinson's disease, hemorrhagic brain damage, etc [26–28]. Furthermore, the ablation of GPX4 in neurons has been demonstrated to cause motor neuron degeneration and paralysis [29]. However, the relevance of GPX4 and phospholipid peroxidation-induced neuronal damage to ALS is still unclear. In this study, we report the phenotypic significance of GPX4 deficiency and the accumulation of phospholipid peroxides in the spinal cord of *SOD*^{G93A} mice. Besides, intrathecal injection of neuron-targeted *GPX4* and the treatment of phospholipid peroxidation inhibitor, ferrostatin 1 (Fer-1), significantly attenuated motor dysfunction in ALS mice. Our findings provide novel insights on a heretofore unknown role for GPX4 deficiency in phospholipid peroxidation during ALS pathogenesis, which may provide new direction for developing novel treatments.

Materials and methods

Chemicals and reagents

Malondialdehyde (MDA) detection kit was purchased from Beyotime (Shanghai, China). NADPH assay kit was obtained from Comin Biotechnology (Suzhou, China). Fer-1 was acquired from Selleck Chemicals (Houston, TX, USA). Primary antibodies against 4HNE (#Ab46545), SOD1 (#Ab16831), NeuN (#Ab104224) and GPX4 (#Ab125066) were purchased from Abcam (Cambridge, UK). Primary antibodies against ChAT (#Ab144P) and NeuN (#ABN78) were obtained from Millipore (Billerica, MA, USA). Primary antibody against GFAP (#3670P) was purchased from Cell Signaling Technology (Beverly, MA, USA). Primary antibodies for GAPDH (#FD0063) and β-Actin (#FD0060) were obtained from Fdbio science (Hangzhou, China). Secondary antibodies including goat anti-rabbit IgG-HRP (#FDR007), goat anti-mouse IgG-HRP (#FDM007) and rabbit anti-goat IgG-HRP (#FD8000) were obtained from Fdbio science. Secondary antibodies including Alex Fluor 594 anti-rabbit (#A-21207), Alex Fluor 488 anti-rabbit (#A-21206) and Alex Fluor 555 anti-mouse (#A-31570) were obtained from Life Technology (Gaithersburg, MD, USA).

Animals

Transgenic male mice with high copy number (20–25 copies, #004435), low copy number (7–10 copies, #002299) of mutant human *SOD1*^{G93A}, and *Gpx4*$^{fl/fl}$ mice (#027964) were obtained from Jackson Laboratory (Bar Harbor, ME, USA). *SOD1*^{G93A} mice were bred with C57BL/6J background female mice obtained from Guangdong Medical Laboratory Animal Center (Guangzhou, China). The mice were genotyped by PCR using DNA extracted from tail biopsies. Littermates were used as controls and the mice used in the experiment were equally male and female. The mice were housed in a room at a mean constant temperature (24 ± 2 °C), a relative humidity of 50–60%, and provided free access to standard pellet chow and water under a 12-h light-dark cycle.

Ethics statement

All animal experiments were performed in accordance with the National Institutes of Health's Guide for the Care and Use of Laboratory Animals (NIH publication No. 80-23, revised in 1996) and were approved by the Animal Ethics Committee of Jinan University (Approval Number: 20130904001).

Intrathecal injection

Intrathecal injection was done under sterile conditions and performed as previously described [30,31] with minor modifications. Fer-1 (5 mg/mL, 10 μL), a total of 3×10^{10} particles of adeno-associated virus (AAV) serotype 2/9 vector carrying genetically encoded homo sapiens glutathione peroxidase 4 (*GPX4*, ref. seq. NM_002085.5) or *Cre-EGFP* under the hSyn promoter (BrainVTA, Wuhan, China) were intrathecally injected in a 10 μL volume using a Hamilton syringe. Briefly, mice were anesthetized with 1.25% avertin. The surgical area was shaved and disinfected with iodine tincture. After placing mice on a prone position and de-iodinating with 75% alcohol, the skin was cut to expose the lumbar spine. A Hamilton syringe was perpendicularly inserted into the gap between the L5 and L6 in the lumbar vertebrae. Once contact was made with the bone of the spinal column, the needle angle was reduced to approximately 30° and inserted into the subarachnoidal space. The solution containing AAV or Fer-1 were slowly released into the cerebrospinal fluid when there is a sudden lateral movement or 'S' shape of the tail. The syringe was removed 1 min later to minimize cerebrospinal fluid and vector leakage. After the surgery, animals were housed in a cage with free access to food and water till the end point. Age-matched transgenic and WT littermates were injected with AAV vector or solvent (2% DMSO + 50% PEG300 + 5% Tween 80 + ddH_2O) as controls. Intrathecal injection of Fer-1 into *SOD1*^{G93A} was carried in mice that were about 252–260 days-old. Intrathecal injection of *GPX4*-AAV into *SOD1*^{G93A} mice and *Cre-EGFP*-AAV into *Gpx4*$^{fl/fl}$ were performed in mice that 28.5 weeks and 6.5 weeks-old, respectively. EGFP fluorescent optical images were taken of the stripped spinal cord using an *in vivo* fluorescence imaging system (PerkinElmer, USA).

Behavioral analysis

Motor function was assessed once a week using the rotarod test, wire hanging test and neurological scoring. All animals were pre-trained for three trials before the formal tests of motor function.

For the rotarod test [32], mice were placed onto an accelerating rotating rod (Ugo Basile, Comerio, Italy) with an increasing speed from 5 to 30 RPM within 5 min. The ability of the mouse to stay on the rod without falling was automatically timed by the apparatus. Each mouse was given three trials and the average value was recorded.

The wire hanging test was applied to measure the muscular strength of mice [33,34]. The wire mesh used for this test was 50 × 40 cm consisting of 1.2 mm diameter wires with an interval of 0.8 mm between adjacent in the mesh. The mouse was placed on the center of the wire mesh and then carefully turned over, keeping it 60 cm off the ground. The time taken for the mouse to fall off was recorded. The test was terminated at 180 s for each trial. Each mouse was given three trials and the average value was recorded.

Neurological scoring was measured with reference to a system developed by the ALS Therapy Development Institute [35]. Briefly, the mouse's movement and performance of its hind limbs were recorded. Each mouse is given a maximum score of 4 points when the hindlimb presents a normal splay. A score of 0 is given if the mouse cannot straighten itself within 30 s.

Western blot analysis

Dissected spinal cords from mice were homogenized at 4 °C by sonication in cold lysis buffer (Beyotime, Shanghai, China) containing a protease inhibitor cocktail (Targetmol, Shanghai, China). The supernatant was collected after centrifugation of the homogenate at 12,000 RPM for 10 min at 4 °C, and the protein concentration was measured using BCA protein assay kit (Pierce, Rockford, IL, USA). Protein extracts were separated on 12% SDS polyacrylamide gel and transferred onto polyvinylidene difluoride membranes (Millipore, Billerica, MA, USA). After blocking the membrane with 5% nonfat milk in Tris buffered saline-Tween 20 for 1 h at room temperature, target proteins on the membrane were incubated overnight at 4 °C with the primary antibody. On the second day, the membrane was rinsed with Tris buffered saline-Tween 20 and following incubated with the corresponding secondary antibodies for 2 h at room temperature. Bound antibody was visualized using an ECL system (Tanon 5200, Shanghai, China). Band intensity was quantified using Quantity One software and target protein bands normalized to the housekeeping protein band GAPDH. Results were plotted using GraphPad prism software 8.0.

Measurements of MDA, GSH and NADPH

MDA levels were assessed using the thiobarbituric acid reactive substances assay kit (Beyotime, Shanghai, China) according to the manufacturer's instructions.

GSH content analysis was performed as described in our previous study [15] using a C18 column (4.6 × 150 mm, 5 μm, Cosmosil, Japan) and a four-channel ESA 5600A CoulArry Detector to detect the GSH signal.

NADPH content was assessed using a commercial chemical assay kit (Keming, Suzhou, China) according to the manufacturer's instruction. Briefly, the method was based on the spectrophotometric measurement of the color produced when NADPH reduced oxidized thiazole blue to formazan (570 nm).

Quantitative reverse transcription polymerase chain reaction

Dissected spinal cords from mice were extracted using TRIzol reagent (Thermo Fisher Scientific, Waltham, MA, USA) and RNA concentrations determined using a spectrophotometer (NanoDrop 2000, Thermo Fisher Scientific, Waltham, MA, USA). RNA was transcribed into cDNA (cDNA synthesis kit, TransGen Biotech, Beijing, China). Relative expression of RNA was measured using SYBR green (TransGene Biotech) on a CFXConnectTM reverse transcription (RT) machine (Bio-Rad, Hercules, CA, USA) and calculated using the $2^{-\Delta Ct}$ method. The primer sequences are shown in Supplementary Table S1 and S2.

Tissue processing, Nissl staining, and immunofluorescence

Anesthetized mice were sacrificed and transcardially perfused with saline followed by 4% paraformaldehyde in PBS. The lumbar region (L1–L5) of the spinal cord was isolated and post-fixed in 4% paraformaldehyde overnight at 4 °C, cryoprotected for 48 h in PBS containing 30% sucrose, embedded in O.C.T (TisssueTek, Sakura) and cut at a thickness of 20 μm using a Leica vibratome (Leica Biosystem, Nussloch, Germany).

For Nissl staining, frozen slides were air-dried for 2 h. Sections were immersed in 0.1% (w/v) cresyl violet acetate (MilliporeSigma, Burlington, MA, USA) using a standard protocol, dehydrated and imaged (PreciPointGmbh M8 microscope, Freising, Germany). Nissl-stained motor neurons cells having a diameter at least 25 μm in the ventral horn (VH) were counted.

For immunofluorescent staining, frozen sections were air-dried for 2 h and then blocked with 5% normal donkey serum/0.5% TritonX-100/PBS for 2 h at room temperature. After spinning off the liquid, slides were incubated overnight at 4 °C with the indicated primary rabbit anti-NeuN (Millipore, Bedford, USA) or mouse anti-GFAP (Millipore, Bedford, USA) antibodies diluted in 5% normal donkey serum/0.1% Triton X-100 in PBS. Sections were then washed with PBS and incubated for 2 h at room temperature with an appropriate fluorescent secondary antibody. Cover slips were

mounted over one drop of anti-fade mounting medium (Beyotime, Shanghai, China) and examined under a fluorescent microscope (Zeiss Axio Observer Z1, Carl Zeiss, Oberkochen, Germany). Photographs of GPX4, NeuN and GFAP were analyzed using Image-pro plus 6.0 software.

LC-MS analysis of phospholipids

Lipids in the spinal cord were extracted by the Folch procedure [36] and were further analyzed by LC-MS. Phospholipids were separated on a normal-phase column (Luna Silica (2), 3 μm, 150 × 2. 0 mm (Phenomenex)) at a flow rate of 0.2 mL/min on a DionexUltiMate 3000 HPLC system (Thermo Fisher Scientific). The mobile phase consisted of 10 mM ammonium formate in propanol/hexane/water (285:215:5, v/v/v, solvent A) and 10 mM ammonium formate in propanol/hexane/water (285:215:40, v/v/v, solvent B). The elution gradient program was set as follow: 0 min, 10% B; 20 min, 32% B; 30 min, 70% B; 32 min, 100% B; 58 min, 100% B; 60 min, 10% B; 75 min, 10% B. The column temperature was maintained at 35 °C. The injection volume was 2 μL.

MS analysis of phospholipids was performed on a Q-Exactive Hybrid Quadrupole-Orbitrap mass spectrometer (Thermo Fisher Scientific, Waltham, MA, USA). Analysis was performed in full MS negative mode at resolution setting of 70,000 and data-dependent-MS/MS mode at resolution setting of 17,500. Ion source conditions were set as follows: spray voltage, 3.0 kV; vaporizer temperature, 320 °C; transfer tube temperature, 350 °C; S-lens Rf level, 60; sheath gas, 35 (arbitrary units); auxiliary gas, 15 (arbitrary units); sweep gas, 1 (arbitrary units). For MS, the scan range was *m*/*z* 400–1800 and the maximum ion injection time was 128 ms using 1 microscan per MS scan. For MS/MS, high energy collision induced dissociation analysis was performed with the collision energy set to 24 eV and the maximum ion injection time of 500 ms. An isolation window of 1.5 Da was set for MS/MS scans.

ST analysis

ST is a transcriptomics technology based on *in situ* capture, and the operation steps are described previously [37]. GPX4 gene expression analysis was performed on the large-scale and high-resolution ALS transcriptomics data in the public interactive data browsing website, https://als-st.nygenome.org. The ALS database collected about 1200 mouse lumbar spinal cord tissue samples from4 periods (pre-symptomatic, onset, symptomatic and end-stage) and a total of ∼1200 spinal cord sections of 67 mice. It also collected 80 postmortem sections of lumbar and cervical spinal cord tissues from 7 sporadic ALS patients with lumbar or bulbar-onset.

Resting EMG recording

Resting EMG recording analysis was performed as previous study [38]. Mice were anesthetized with 1.25% avertin and the left hind limbs were shaved. To record EMG potentials, two 30-G platinum transcutaneous needle electrodes were inserted into the gastrocnemius, keeping two recording electrodes ∼2 mm apart. Electrodes were connected to an active head stage and the signal amplified (X100) and digitized using the PowerLab 16/32 data-acquisition system (ADInstruments). The signal within 5 mins was recorded at a sampling rate of 20 kHz and stored in a PC, and then analyzed using LabChart 8.15 (ADInstruments).

MRI and DTI

MRI and DTI analysis were performed as previous research [39]. Paraformaldehyde (4%)-fixed spinal cords from mice were placed in 5 mL Eppendorf tubes and immersed in perfluorocarbon oil media (Fluorinert, FC-40, 3 M). MRI scanning was performed using a Bruker 9.4 T Biospec 9430 USR (Ettlingen, Germany) with a TX Volume Array and RX Surface Array. The diffusion images were acquired by using a spin-echo diffusion weighted sequence with the following acquisition parameters: TR = 3 s, TE = 20 ms, NEX = 8, FOV = 18 mm × 18 mm, matrix size = 108 × 96, and b = 650 s/mm^2). Total imaging time was 14 min. Slice thickness was 0.7 mm. A DTI diffusion scheme was used, 17 sequential imaging sections centered in the lumbar spinal cord and a total of 30 diffusion sampling directions were acquired. The values of fractional anisotropy (FA) and mean diffusivity (MD) were calculated by ParaVision 360 V1.1. Volume analyses were performed by manually segmenting the boundary between the gray matter (GM) and the white matter (WM), slice by slice, using Carimas 2.9 RayVisualization v.2.9.4.0 (Turku PET Centre). The total volumes of GM and WM around lumbar 3–5 enlargement (3.5 mm spinal cord length) were counted.

Statistics

Data were analyzed using Graphpad 8.0 software and expressed as the mean ± SEM. Differences among groups were determined by either Student's *t* test or One-way ANOVA or Two-way ANOVA. $P < 0.05$ was considered statistically significant.

Study approval

All animal experiments were performed in accordance with the National Institutes of Health's Guide for the Care and Use of Laboratory Animals (NIH publication No. 80-23, revised in 1996) and were approved by the Animal Ethics Committee of Jinan University (Approval Number: 20130904001).

Results

Accumulation of phospholipid peroxides is an essential feature in ALS mice

The G93A mutation of *SOD1* is an inherited ALS causative factor, which produces toxic SOD1 protein aggregates and contributes to the pathogenesis of ALS [40]. In order to explore the relationship between phospholipid peroxidation and ALS disease progression, low copy (∼8 copies) and high copy (∼25 copies) mutated *SOD1*^{G93A} (hereinafter referred to as G93A) mouse strains with different speeds of the occurrence and development of ALS [41] were utilized in this study. Firstly, the impact of high- and low-copy G93A on motor function in mice were evaluated by behavioral tests for 35 weeks. The rotarod test (Fig. 1a), wire hanging test (Supplementary Fig. S1a), and neurological scores (Supplementary Fig. S1b) showed that the average age of disease onset of high copy and low copy mice was ∼12 weeks and ∼28 weeks, respectively, and the average age of disease endpoint was ∼21 weeks and ∼35 weeks, respectively. These observations suggest that increased copy number of G93A mutation led to an earlier onset of motor dysfunction. Since the loss of motor neurons in the lumbar spine is one of the key pathological features of ALS, the motor neurons in ventral horn (VH) of lumbar spine were marked using NeuN and Nissl staining. The results show that when compared with WT group, the motor neurons in G93A mice were significantly shrunken (Fig. 1b and 1c). Also, the number count decreased as the copy number increased (Fig. 1d and 1e).

To delineate the relationship between phospholipid peroxidation and G93A mutation, we generally assessed the levels of phospholipid peroxides in ALS, concentrations of two important

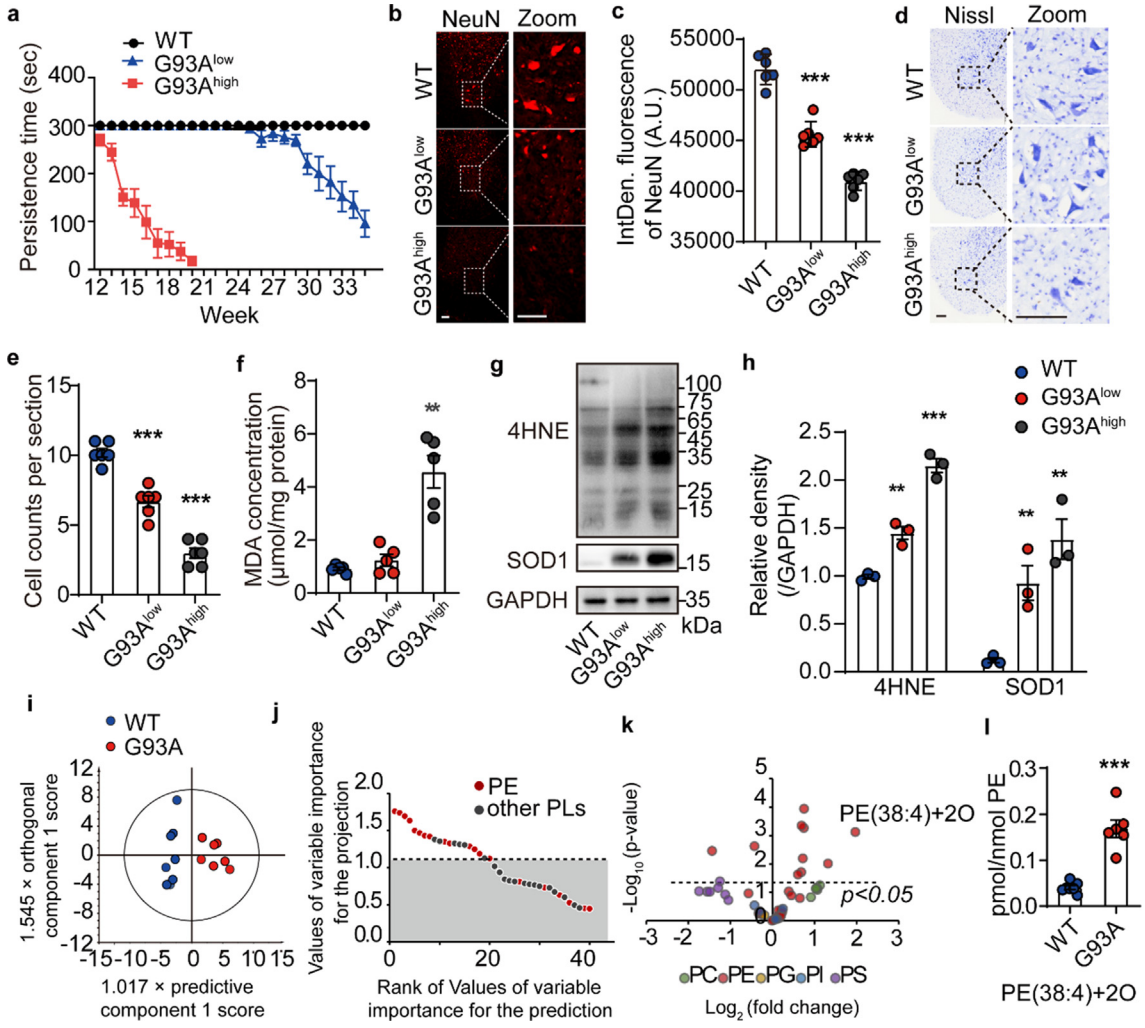

Fig. 1. The number of motor neuron decreased and the phospholipid peroxides increased with the accumulation of *SOD1*^{G93A} transgene copy number. **a** Persistence time of mice on the rotating rod. $N_{WT,\ G93A\text{-}low} = 6$. $N_{G93A\text{-}high} = 8$. **b, c** Representative images and integrated fluorescence density of NeuN-stained motor neurons in the lumbar ventral horn (VH) of the spinal cord at the terminal age of G93A mice. Scale = 100 μm. **d, e** Representative Nissl staining images and corresponding quantification of large motor neurons in the lumbar VH of the spinal cord at the terminal age of G93A mice. Scale = 100 μm. $N = 6$. **f** MDA concentration in the spinal cord of mice at 120 day. $N = 5$. **g, h** Western blotting and quantifications of 4HNE and SOD1 in the spinal cord of mice at 120 day measured by Western blotting. $N = 3$. **i** Multivariate statistical analysis of oxidative phospholipids using orthogonal partial least squares–discriminate analysis. **j** Values of variable importance for the projection of oxidative phospholipids. **k** Volcano plot of oxidative phospholipids represented by $\log_2$ (fold change) of G93A 120 day/WT 120 day groups plotted against the $-\log_{10}$ (p-value). Statistical significance was evaluated by t test ($p < 0.05$). **l** Amount of PE(38:4) + 2O in G93A 120 day and WT 120 day mice. $N_{WT} = 7$. $N_{G93A} = 6$. Data are represented as mean ± SEM, $^{**}p < 0.01$, $^{***}p < 0.001$ *vs.* WT group by t test.

phospholipid peroxidation end-products, malondialdehyde (MDA) and 4HNE in the spinal cords of 120-day-old high copy and low copy G93A mice were measured. As shown in Fig. 1f-h, MDA and 4HNE levels increased with a higher transgene copy number. Also, the mutant SOD1 was significantly up-regulated in 120-day-old high copy G93A mice corresponding to the mid-stage state of ALS disease (Fig. 1f-h).

Further, LC-MS/MS-based redox phospholipidomics analysis was performed to determine the molecular species of oxidized phospholipids, focusing on the five major categories of phospholipids in WT and G93A low copy mice, including PE, phosphatidylcholine (PC), phosphatidylinositol (PI), phosphatidylserine (PS), and phosphatidylglycerol (PG). As shown in Fig. 1i, the composition of oxidized phospholipids in G93A mice was significantly different from that in WT mice. Among the five phospholipids discussed above, oxidized PEs were found to be primary contributors to this difference (Fig. 1j). Interestingly, oxidized arachidonic acid-PE (PE(38:4) + 2O), a ferroptosis-specific cell death signal [22], showed the most significant elevation (Fig. 1k and 1 l). These data appear to reveal the accumulation of PE peroxides as a major characteristic feature in the pathogenesis of ALS.

Inhibition of phospholipid peroxidation alleviates motor dysfunction and neuron loss of ALS mice

In order to evaluate the potential role of phospholipid peroxidation-induced injury in ALS, Fer-1, a specific inhibitor of lipid peroxidation was intrathecally injected (5 mg/mL, 10 μL) into the L5-L6 lumbar spine of symptomatic low copy G93A mice on day 252 and day 260, respectively (Fig. 2a). As shown by the rotarod test, wire hanging test and neurological scores (Fig. 2b-d), Fer-1 administration significantly mitigated behavior deficits in G93A mice. Meanwhile, the contents of MDA and 4HNE in the spinal cords were also significantly reduced in Fer-1 treated animals, comparing with G93A group (Fig. 2e-g). These data indicate that the restriction of phospholipid peroxidation in the spinal cord can improve the motor performance of ALS mice. Furthermore, the damage of motor neuron caused by G93A mutation was examined.

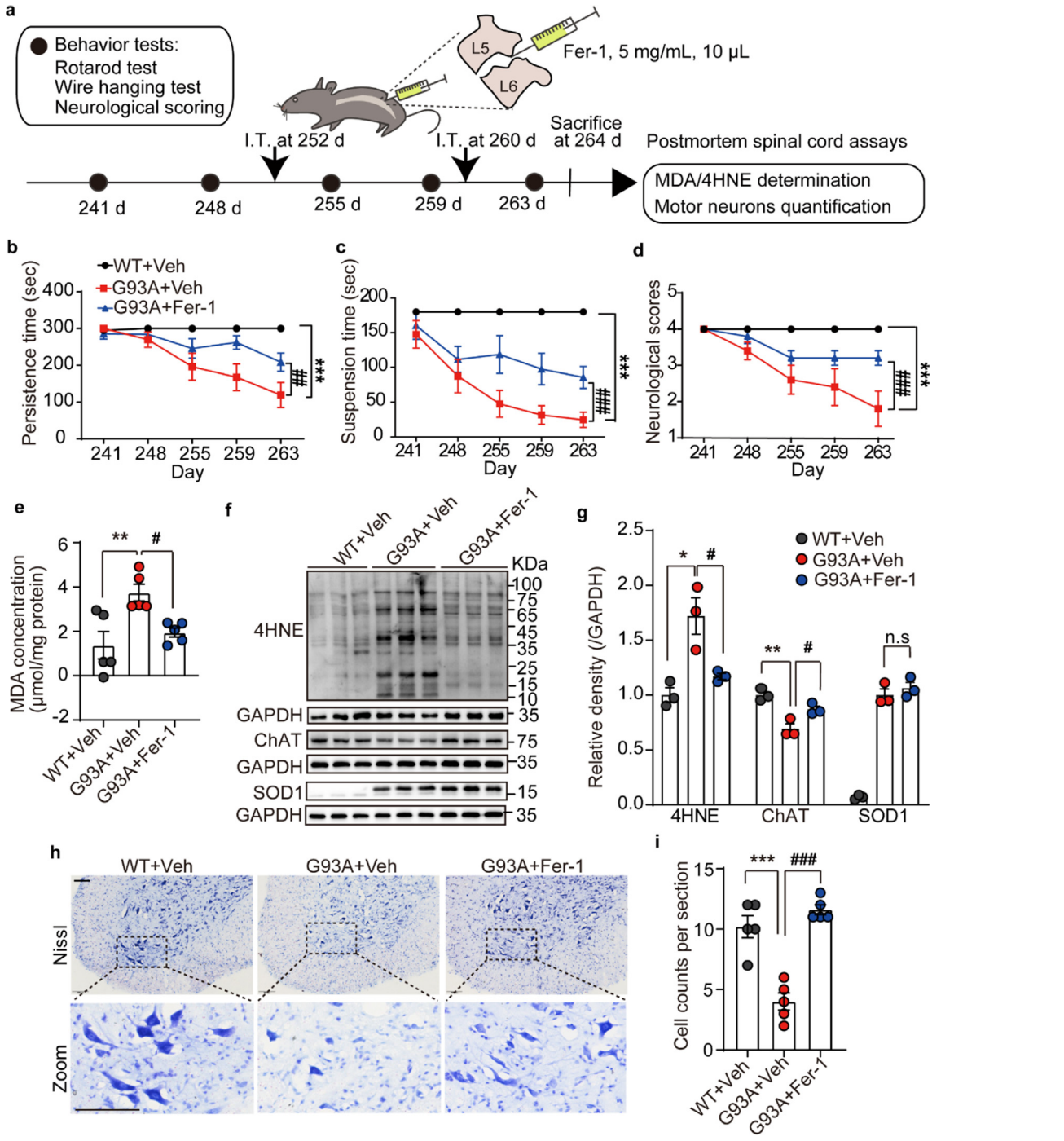

Fig. 2. Lipid peroxidation inhibitor Fer-1 alleviated motor dysfunction and neuron loss of G93A mice. **a** Schematic diagram of Fer-1 administration, behavior test and 'postmortem' assays. **b-d** Persistence time on the rotating rod, the hanging time on the wire mesh, and statistics of neurological scores of G93A mice intrathecally injected with Fer-1. Data are represented as mean ± SEM. $N = 5$ mice per group, $^{***}p < 0.001$ G93A + Veh *vs.* WT + Veh group; $^{\#\#}p < 0.01$, $^{\#\#\#}p < 0.001$ G93A + Fer-1 *vs.* G93A + Veh group by Two-way ANOVA. **e** MDA concentration in the spinal cord of mice. $N = 5$. **f, g** Western blotting and band quantifications of 4HNE, ChAT and SOD1 in the spinal cord of mice. $N = 3$. **h, i** Representative Nissl staining images and quantification of the large motor neurons in the lumbar VH of the spinal cord of mice. Scale = 100 μm. $N = 5$. Data are represented as mean ± SEM, $^{*}p < 0.05$, $^{**}p < 0.01$, $^{***}p < 0.001$ G93A + Veh *vs.* WT + Veh group; $^{\#}p < 0.05$, $^{\#\#}p < 0.01$, $^{\#\#\#}p < 0.001$ G93A + Fer-1 *vs.* G93A + Veh group by One-way ANOVA. I.T.: intrathecal injection; Veh: vehicle; Fer-1: ferrostatin 1.

The protein expression of a motor neuron marker ChAT was increased in Fer-1 treated ALS mice (Fig. 2f and 2 g). Consistent with this, the results of Nissl staining also showed that Fer-1 could restore the decrease of large motor neurons (>25 μm) in the VH of the lumbar spinal cord of G93A mice (Fig. 2h and 2i). This is a very interesting observation since it suggests that inhibition of lipid peroxidation is upstream to motor neuron loss in ALS. This raises the inspiring possibility of therapeutic options directed at preventing phospholipid peroxidation in the spinal cord in an effort to delay the progression of ALS.

GPX4 expression is impaired in ALS mice and patients

The reasons for increased phospholipid peroxidation in ALS animals could be either, an accumulation of membrane phospholipid peroxides or a reduction in antioxidant capacities such as GPX4

activity [42]. To analyze the contribution of phospholipid peroxidation-related genes to ALS, comparative qPCR analysis was performed using spinal cord extracts from WT and G93A transgenic animals. As shown in Fig. 3a, the expression levels of genes that promote phospholipid peroxidation (*Lpcat3*, *Ncoa4*, *Tfrc*, *Alox15*, *Acsl4*, *Alox5*, *Alox12*, *Dmt1*, *Ptgs2*) increased, while genes that can reduce phospholipid peroxidation (*Gpx4*, *Slc7a11*) decreased in the spinal cord of ALS mice. Among them, GPX4, a key antioxidant enzyme that is known to contribute to maintenance of redox balance in phospholipid [43], was significantly under-expressed in the spinal cords from ALS mice (Fig. 3a).

Next, we utilized an interactive data exploration portal for the spatiotemporal transcriptome atlas of the ALS spinal cord (https://als-st.nygenome.org) to perform precise spatial gene expression analysis of *Gpx4* in ALS spinal cord samples derived from both human and mice. Spatial transcriptomics (ST) is a transcriptomics technology based on *in situ* capture, which accurately correlates RNA-seq data with spatial information through specific sequence barcodes, so as to quantify and visualize the transcriptomics of tissue sections in space. The principle of ALS ST is showed in the Fig. 3b. As shown in Fig. 3c, *Gpx4* gene expression in G93A mice at the age of 120 days was lower compared to WT control mice. Spatially, the decrease of *Gpx4* gene expression occurred in the ventral horn (VH) region (Fig. 3d) as well as other areas of the lumbar spine (Supplementary Fig. S2).

ALS patients can be categorized into lumbar-onset and bulbar-onset. By comparing the *GPX4* gene expression in the lumbar spinal cord of ALS patients with lumbar onset and bulbar onset, one can determine the difference between the onset and non-onset sites. Analysis of lumbar spine sections from ALS patients using the ST database revealed that the level of *GPX4* gene in the VH of onset site was lower than that in the non-onset site (Fig. 3e), thereby

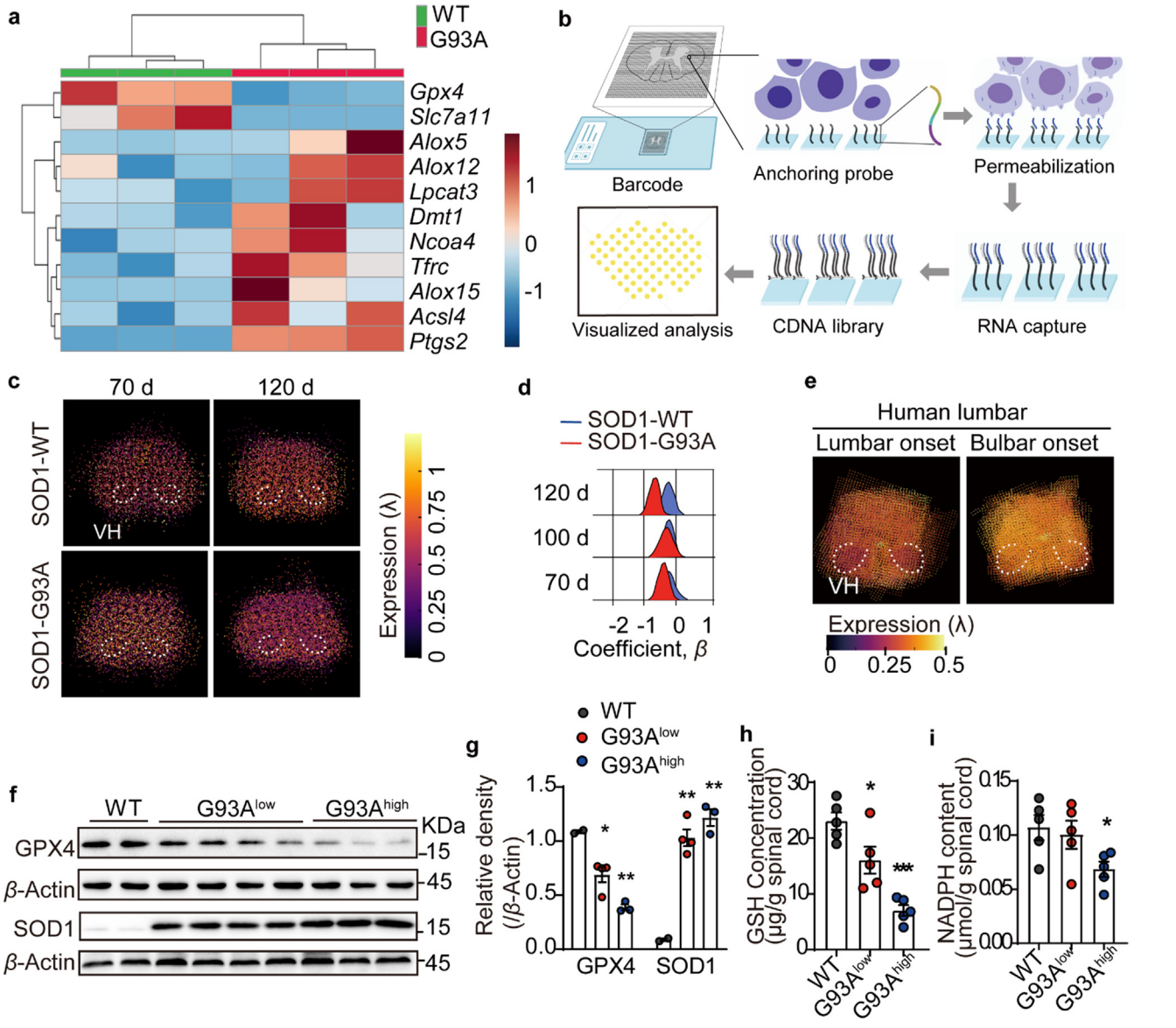

Fig. 3. GPX4 was down-regulated in the spinal cord of both G93A mice and ALS patients. **a** Lipid peroxidation-related genes expression in the spinal cord of mice at 120 day detected by qPCR, and expressed using a heatmap. $N = 3$ mice each group. **b** Schematic diagram of spine spatial transcriptomics. **c, d** Spatial transcriptomics representative images of *Gpx4* gene expression in the lumbar spine and statistics of the coefficient parameter β of *Gpx4* gene in the lumbar VH of the spinal cord at 70,100 and 120 days age-matched G93A mice and WT mice. **e** Spatial transcriptional expression of *GPX4* in the lumbar VH of the spinal cord of ALS patients with lumbar onset and bulbar onset. **f, g** Protein expression and quantifications of GPX4 and SOD1 in the spinal cord of G93A high copy, low copy mice and WT littermates at 120 days age. **h, i** GSH concentration and NADPH content in the spinal cord of mice at 120 day. Data are expressed as mean ± SEM. $N = 5$ mice each group, $^{*}p < 0.05$, $^{***}p < 0.001$ *vs.* WT group by *t* test. VH: ventral horn.

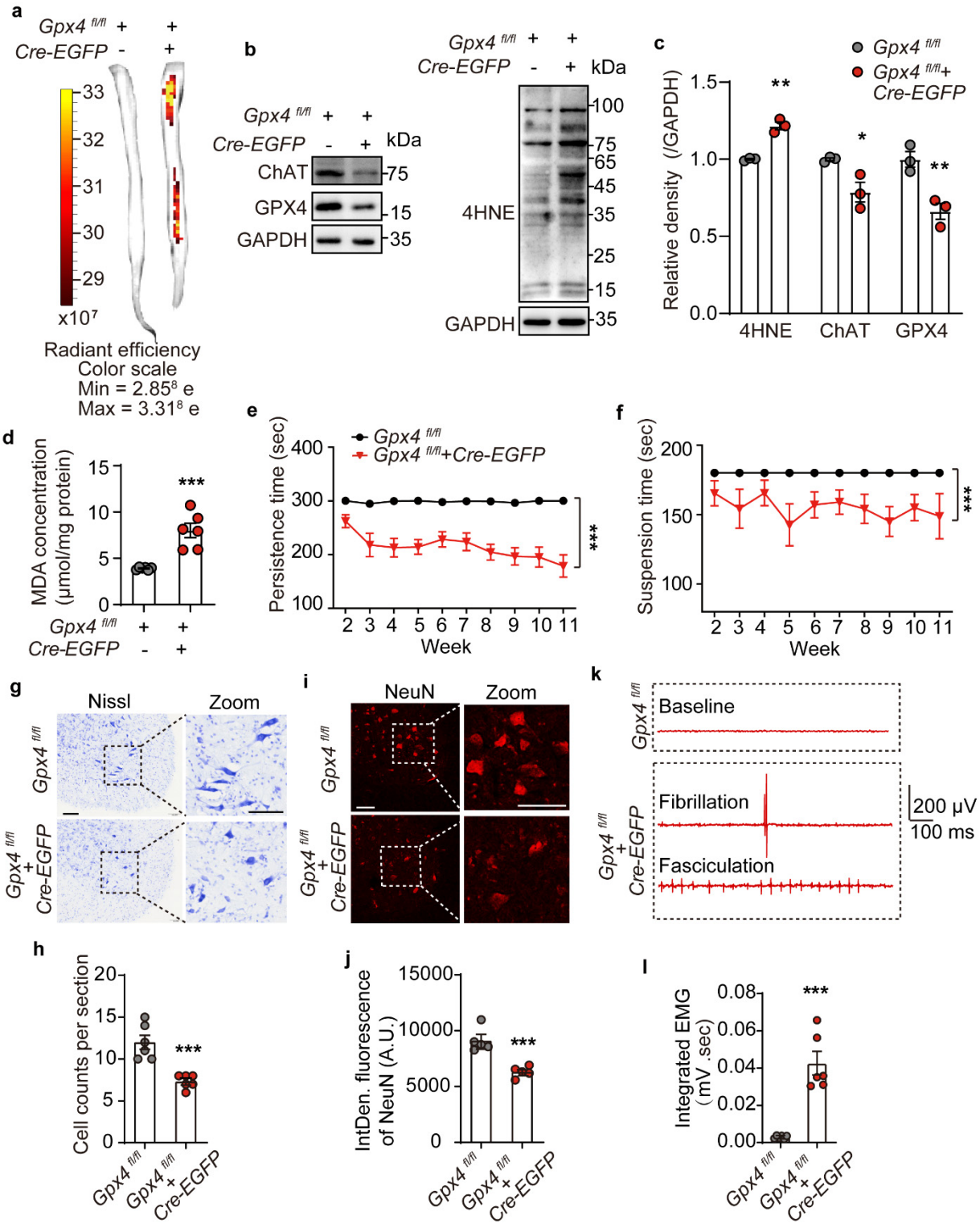

Fig. 4. Intrathecal *Gpx4* knockdown induced sever motor performance deficits in mice. **a** Fluorescence imaging of the isolated spinal cord of *Gpx4*$^{fl/fl}$ mice intrathecally injected with *Cre-EGFP*-AAV under the hSyn promoter. The red/yellow gradient scale indicates the intensity of EGFP signal. **b, c** Expression levels and quantifications of GPX4, ChAT and 4HNE in the spinal cord of mice. *N* = 3 mice each group. **d** MDA concentration in the spinal cord. *N* = 6 mice each group. **e, f** Persistence time on the rotating rod and suspension time on the wire mesh of mice. Data are represented as mean ± SEM. *N* = 6 mice per group, $^{***}p < 0.001$ *Gpx4*$^{fl/fl}$ + *Cre-EGFP vs. Gpx4*$^{fl/fl}$ by Two-way ANOVA. **g**, **h** Representative Nissl staining images and quantification of the large motor neurons in the lumbar VH. *N* = 6. **i, j** Representative images and integrated fluorescence density of NeuN-stained motor neurons in the lumbar VH. *N* = 5. **k** EMG activity and the presence of fibrillation and fasciculation in the GCM of *Gpx4*$^{fl/fl}$ mice treated with *Cre-EGFP*-AAV or AAV before sacrifice. **l** Quantitative analysis of the integrated EMG signals. *N* = 6 mice each group. Data are expressed as mean ± SEM, $^{*}p < 0.05$, $^{**}p < 0.01$, $^{***}p < 0.001$ *Gpx4*$^{fl/fl}$ + *Cre-EGFP vs. Gpx4*$^{fl/fl}$ by *t* test. EMG: electromyography; GCM: gastrocnemius muscle. (For interpretation of the references to color in this figure legend, the reader is referred to the web version of this article.)

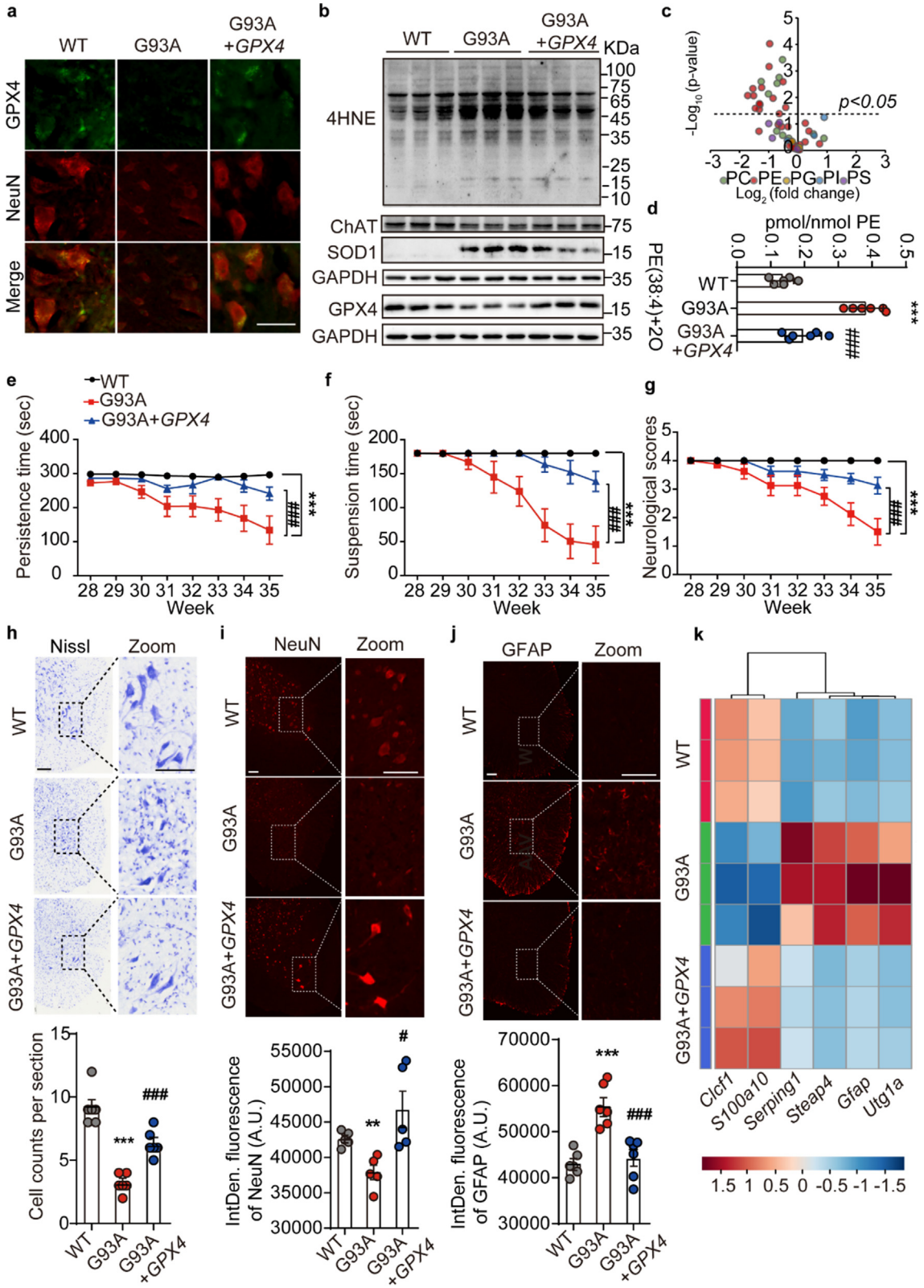

Fig. 5. Intrathecal overexpressing *GPX4* rescued motor performance disorder in G93A mice. **a** Representative fluorescence co-localization images of GPX4 and NeuN in the lumbar ventral horn. Scale = 50 μm. *N* = 3. **b** Expression of GPX4, ChAT, and 4HNE in the spinal cord of mice. *N* = 3. **c** Volcano plot of oxidative phospholipids represented by $\log_2$ (fold change) of G93A + *GPX4*-AAV/G93A + AAV groups plotted against the $-\log_{10}$ (*p*-value). Statistical significance was evaluated by *t* test ($p < 0.05$). **d** Amount of PE (38:4) + 2O in the spinal cord of mice. *N* = 6. **e-g** Persistence time on the rotating rod, suspension time on the wire mesh, and statistics of neurological scores of mice intrathecally injected with *GPX4*-AAV. Data are represented as mean ± SEM. *N* = 6 mice each group, $^{***}p < 0.001$ G93A + AAV *vs.* WT + AAV group; $^{\#\#\#}p < 0.05$ G93A + *GPX4*-AAV *vs.* G93A + AAV group by Two-way ANOVA. **h** Representative Nissl staining images and quantification of motor neurons in the lumbar VH. *N* = 6. **i** Representative images and the integrated fluorescence density of NeuN-stained motor neurons in the lumbar VH at the terminal age. *N* = 5. **j** Representative images and the integrated fluorescence density of GFAP-stained astrocytes in lumbar VH at the terminal age. Scale = 100 μm. *N* = 6 mice each group. **k** Pan (*Gfap*, *Steap4*), A1 (*Serping1*, *Utg1a*) and A2 (*Clcf1*, *S100a10*) astrocyte genes expression in the spinal cord of mice detected by qPCR, and expressed using a heatmap. *N* = 3. Data are expressed as mean ± SEM, $^{**}p < 0.01$, $^{***}p < 0.001$ G93A + AAV *vs.* WT + AAV group; $^{\#}p < 0.05$, $^{\#\#\#}p < 0.001$ G93A + *GPX4*-AAV *vs.* G93A + AAV group by One-way ANOVA.

providing proof of clinical relevance linking the reduction in *GPX4* with ALS. Similarly, western blot analysis from spinal cords extracts showed a significant reduction in GPX4 protein expression in ALS mice, likely due to the presence of the mutant *SOD1* protein (Fig. 3f and 3 g).

The lipid peroxides-clearing function of GPX4 depends on the small antioxidant molecular GSH. GPX4 converts reduced GSH to oxidized glutathione (GSSG) while reducing lipid hydroperoxides. GSSG is then recycled back to GSH by the actions of glutathione reductase and nicotinamide adenine dinucleotide phosphoric acid (NADPH) [44]. Hence, GSH and NADPH play critical roles in maintaining the function of GPX4 to prevent phospholipid peroxidation. Interestingly, there is a significant decreased in the levels of both GSH and NADPH in the spinal cords of high copy ALS mice (Fig. 3h and 3i), implying a deficiency of GPX4 function. Taken together, the above data reveal impaired GPX4 expression in ALS that likely leads to accumulation of peroxidized phospholipids in the spinal cord.

Intrathecal GPX4 deficiency drives pathological features of ALS in mice

To address the role of GPX4 in ALS, a conditional knockdown mouse model for the *Gpx4* gene was established (*Gpx4* CKD) by intrathecally injecting neuronal-targeted *Cre-EGFP*-AAV under the

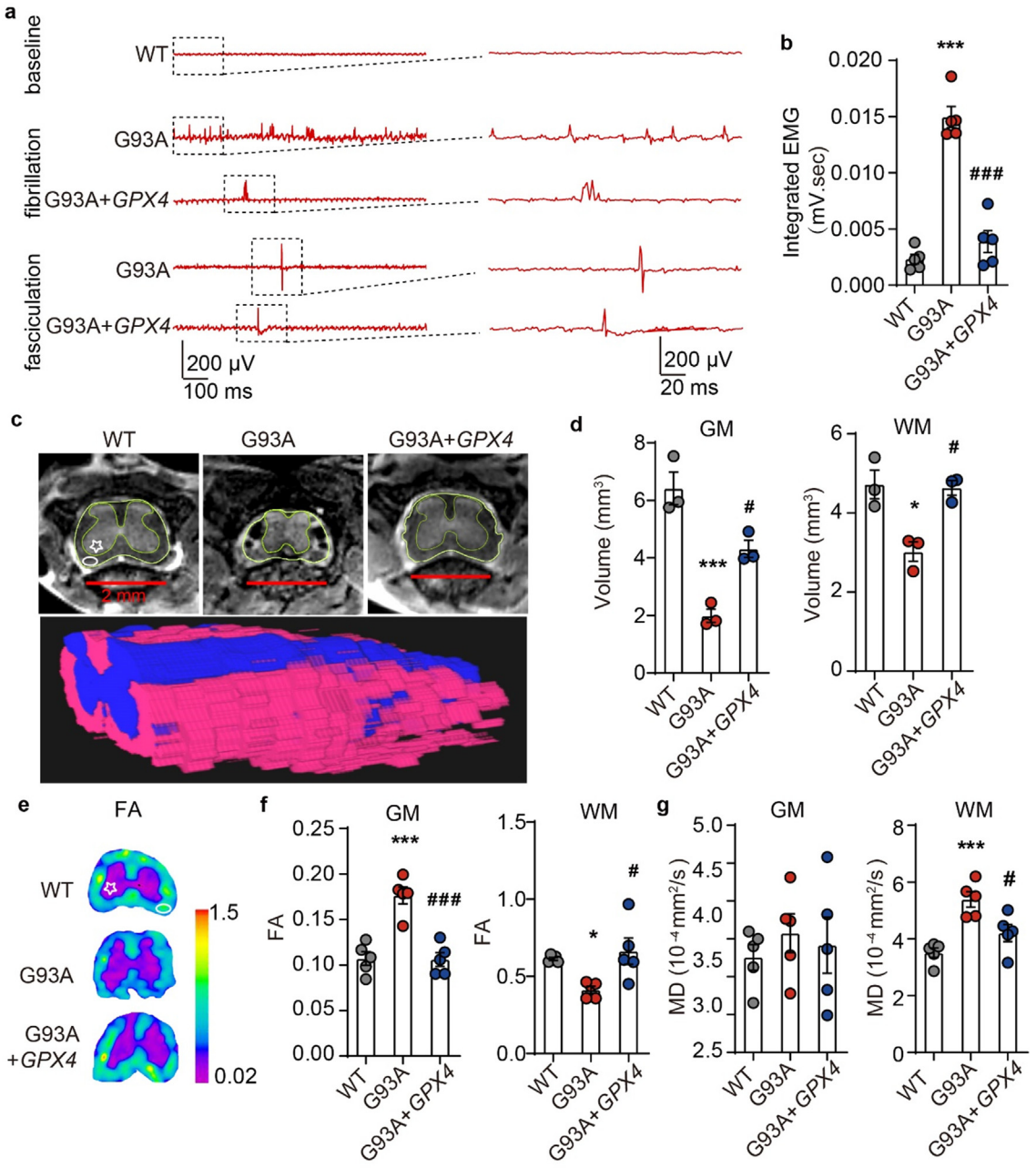

Fig. 6. Intrathecally overexpressing GPX4 in *SOD1*^{G93A} mice improved the GCM fibrillation and fasciculation, and blocked spine atrophy. **a** Fibrillation and fasciculation recordings in the GCM of G93A mice administrated with AAV and *GPX4*-AAV. **b** Quantitative analysis of the integrated EMG signals. *N* = 5 mice each group. **c, d** Representative MRI images and volume analysis of the lumbar GM region and the lumbar WM region. *N* = 3 mice each group. **e** Representative FA maps of lumbar spinal cord. Colors represent FA values, where on pink & purple shows lower FA values and on blue & cyan displays higher FA values. **f, g** Quantitative values of FA and MD in the GM and WM of lumbar VH. *N* = 5 mice each group. Data are represented as mean ± SEM. $^{*}p < 0.05$, $^{***}p < 0.001$ G93A + *EGFP*-AAV *vs.* WT + *EGFP*-AAV group; $^{\#}p < 0.05$, $^{\#\#\#}p < 0.001$ G93A + *GPX4*-AAV *vs.* G93A + *EGFP*-AAV group by One-way ANOVA. FA: fractional anisotropy, MD: mean diffusivity. WM: white matter, indicated by ellipse. GM: gray matter, indicated by pentagram. (For interpretation of the references to color in this figure legend, the reader is referred to the web version of this article.)

hSyn promoter (3×10^{10} particles, 10 μL) into the spinal cord of 6-weeks-old *Gpx4*$^{fl/fl}$ mice. Fluorescence imaging of the isolated spinal cord showed that the *Cre-EGFP*-AAV successfully infected the mouse spinal cord and expressed fluorescent EGFP protein 12 weeks after the intrathecal injection (Fig. 4a). Western blot analysis of these spinal cord extracts showed that protein expression of GPX4 and ChAT was reduced post *Cre-EGFP*-AAV infection (Fig. 4b and 4c). Additionally, 4HNE and MDA levels were significantly elevated in the post infection spinal cords (Fig. 4b-d), indicating that the loss of GPX4 led to lipid peroxidation.

To test whether *Gpx4* CKD in spinal cord neurons led to motor dysfunction, the rotarod test and wire hanging test were performed every week after intrathecal injection of *Cre-EGFP*-AAV. In line with the results obtained from G93A mice, *Gpx4* CKD led to an apparent deficit in persistence time on the rotating bar (Fig. 4e) and wire mesh (Fig. 4f). To demonstrate the effect of GPX4 on the survival of motor neurons, we employed Nissl staining and NeuN immunofluorescence and results showed that *Gpx4* deficiency resulted in a loss of large motor neurons in the lumbar VH of these spinal cords (Fig. 4g-j). To further assess the motor neuron damage caused by loss of GPX4 in the spinal cord, electromyography (EMG), an electro-diagnostic medicine technique was employed to evaluate muscle function in these animals. The resting EMG images of the gastrocnemius muscles (GCM) showed acute fibrillation and fasciculation in *Gpx4* CKD mice when compared to controls, which remained at the baseline (Fig. 4k). Moreover, the integrated EMG signals in the GCM of *Gpx4* CKD mice were remarkably higher than that of control mice (Fig. 4l), suggesting that the loss of GPX4 function in neurons led to the denervation of the muscle through neuron death (Fig. 4g-j). In sum, the deficiency of *Gpx4* in mouse spinal cord neurons leads to neuronal death through lipid peroxides accumulation, resulting in pathological features similar to ALS.

Neuron-targeted GPX4-AAV delivery improves the pathological characteristics of ALS mice

To explore whether restoring GPX4 could alleviate ALS, neuron-targeted *GPX4*-AAV under the hSyn promoter (3×10^{10} particles, 10 μL) was intrathecally injected into the spinal cords of low copy G93A mice at the early stage of disease onset (28.5 w). Firstly, GPX4 was successfully expressed in the spinal cord neurons of G93A mice as confirmed by immunofluorescence co-localization of GPX4 and NeuN (Fig. 5a) and western blotting (Fig. 5b). Secondly, GPX4 expression significantly inhibited the accumulation of phospholipid peroxidation end product 4HNE and prevented the loss of the neuronal marker ChAT compared to G93A mice (Fig. 5b). Further, oxidized phospholipidomics results demonstrated that the accumulation of phospholipid peroxides represented by PE(38:4) + 2O in G93A mice could be reversed by administering *GPX4*-AAV (Fig. 5c and 5d, Supplementary Fig. S3). We also determined that GPX4 expression in G93A mice significantly improved the motor performances compared to G93A mice (Fig. 5e-g). Additionally, loss of Nissl-reactive and NeuN-positive large motor neurons in the lumbar VH of G93A mice was reversed by intrathecally *GPX4*-AAV injection (Fig. 5h and 5i).

In addition to monitor the changes of motor neurons, the status of astrocytes is sensitive to redox states and its activation has been deemed as one of the main pathological characteristics in the progression of ALS [45,46]. To clarify the relationship between GPX4 and astrocytes, we firstly performed immunofluorescence analysis of astrocyte marker GFAP in the spinal cord sections. The images showed that GPX4 overexpression by AAV delivery decreased the number of GFAP-positive cells in the lumbar spine of G93A mice (Fig. 5j). On the other hand, gene profile of pan, type A1 and A2 astrocyte markers was also determined to assess the activation of astrocytes in *GPX4*-AAV treated mice. Results showed that GPX4 overexpression remarkably reduced the expressions of pan (*Gfap*, *Steap4*) and protective A1 (*Serping1*, *Utg1a*) astrocyte signature genes, whereas upregulated the mRNA level of neuro-protective A2 astrocyte marker genes, including *Clcf1 and S100a10* in G93A mice (Fig. 5k). These findings provide primary evidences linking the lack of GPX4 and the activation of astrocytes.

Furthermore, the therapeutic effect of intrathecally *GPX4*-AAV delivery was confirmed by EMG, MRI and diffusion tensor imaging (DTI) detection. EMG examination suggested that *GPX4*-AAV decreased the frequency of fibrillation and fasciculation in the GCM of ALS mice (Fig. 6a). Correspondingly, total EMG signals were significantly attenuated (Fig. 6b), demonstrating an overall improvement in neuromuscular connections following *GPX4*-AAV administration to G93A ALS mice. MRI and DTI are important clinical imaging techniques used in diagnosis of ALS. They were performed to unveil the changes in the volume of the lumbar spine and the pathological changes of lumbar white matter (WM) and gray mater (GM) in ALS mice. Structure and volume analysis based on MRI showed that both the GM and the WM volumes of lumbar spine of sham-operated G93A mice were significantly reduced compared with sham-operated WT mice, and were rescued by *GPX4*-AAV administration (Fig. 6c and 6d), suggesting the positive effect of *GPX4*-AAV delivery on spinal atrophy in ALS mice.

DTI provides quantitative parameters of fractional anisotropy (FA) and mean diffusion (MD), which can evaluate the anisotropy and diffusion of water molecules in the WM and GM of mice spine to reveal the integrity of neuronal pathways. An increase of FA in the GM region and a reduction of FA in the WM region of lumbar VH indicated a loss of neuronal pathway integrity in G93A mice, which was significantly reversed by *GPX4*-AAV administration (Fig. 6e and 6f). Moreover, MD in the WM region increased in the VH of sham-operated G93A mice, also indicating a loss of neuronal pathway integrity, which was attenuated by administration of *GPX4*-AAV, while MD in the GM region remained unchanged (Fig. 6g).

Discussion

ALS is a fatal neurodegenerative disease that results in the progressive loss of motor neurons in the spinal cord and brain. Due to the complexity of the disease pathogenesis, there is still a lack of effective treatments [47,48]. Hence, it is urgent to obtain a better understanding of the molecular mechanism underlying disease progression in ALS, with a focused goal of identifying new therapeutic strategies. Here, we report that the accumulation of phospholipid peroxidation products, represented by doubly-oxygenated arachidonic acid-containing PEs(38:4), due to G93A mutation of *SOD1*. Since PUFA-enriched PEs are essential phospholipids on the double layer of the cell membrane with a rapid turnover rate [49,50], the oxidation of PEs(38:4) is likely to affect the cell membrane function. In fact, an elevation in lipid peroxides and the rupture of the motor cortex plasma membrane have been previously observed in ALS patients and mice [51,52]. As expected, intrathecal injection of lipid peroxidation inhibitor Fer-1 significantly reduced motor neuron loss and improved the motor dysfunction of ALS mice, proposing that anti-phospholipid peroxidation agents might be potential ALS treatment. Our data identified phospholipid peroxidation as an essential feature of the onset and progression of ALS.

One possible explanation for the accumulation of phospholipid peroxides is the impaired antioxidant pathways. GPX4 is a well-known antioxidant enzyme that can directly reduce phospholipid peroxides [42,53]. Our results showed that GPX4 expression in the spinal cord of ALS mice was significantly declined, which has

been confirmed by the spatial gene expression in patients' spinal cord samples from clinical ST database of ALS. Consistently, the conditional knockdown of *Gpx4* was demonstrated to enhance the level of phospholipid peroxidation in the spinal cord and impair mice motor capacity. This result was supported by the study of Chen et al., which has reported that the absence of neuronal GPX4 led to the degeneration of motor neurons and onset of paralysis [29].

During ALS, the activation of astrocytes, the immune cells in the CNS, contributes to the disease progression by promoting inflammation and motor neuron death [54,55]. Activated astrocytes are divided into pro-inflammatory AI and protective A2 types [56]. Thus, we attempted to clarify the relationship between GPX4 and astrocyte activation. Our results demonstrated that the inhibition of GPX4 expression induced by $SOD1^{G93A}$ led to astrocyte activation in G93A ALS mice. Interestingly, we found that the activation of neurotoxic type A1 astrocytes in the ALS spinal cord was attenuated by neuron-targeted overexpression of GPX4 while aggravated by knockdown of GPX4. In fact, apart from the activation, the amount of astrocytes was also affected by GPX4 level, reflected by GFAP immunostaining the spinal cord sections (Fig. 5j, Supplementary Fig. S4). These primary observations gave us a hint that GPX4 might play a key role in maintaining brain immune homeostasis. Since we had previously reported that PE(38:4) + 2O expressed on the surface of ferroptotic cells facilitated their elimination by phagocytosis [57], we speculate that PE peroxides resulted from GPX4 deficiency might also act as signals to activate astrocytes, possibly through the transfer of lipid peroxides from neurons to astrocytes [58]. The deep and exact mechanism is worthy of further investigation.

In this study, we also provide strong evidence for the applicability of *GPX4*-related treatment as a promising therapy for ALS, as neuron-targeted *GPX4*-AAV delivery prohibited phospholipid peroxidation and improved the viability of motor neurons. In addition to AAV delivery system, tetrahedral framework nucleic acids (tFNAs) are also another optimistic choice to deliver exogenous *GPX4*. tFNAs are novel nucleic acid nanoparticles with neuroprotective and anti-inflammatory advantages. Since the tFNAs are beneficial for cell proliferation and can freely pass across cell membranes, they are showing promising applications in the field of ALS therapy [59,60]. However, in the road of developing new drug transport carriers, many obstacles are emerging, such as low resistance to *in vivo* degradation. At all events, the best therapeutic route against ALS by targeting GPX4 is in need of further exploration.

Although the present study has revealed the critical role of GPX4 in the pathological changes of ALS and defined its potential as therapeutic target, the specific molecular mechanism by which G93A inhibits GPX4 expression warrants further investigation. It has been reported that the expression and activity of GPX4 are under the control of selenium or GSH [61,62]. At the transcriptional level, the *GPX4* mRNA level can be regulated by selenium *via* the transcription factor AP-2 gamma and the specific protein 1 [63,64]. At the post-transcriptional modification level, alternative splicing of the GPX4 mRNA joint linker based on different signal stimuli or developmental stages is a factor that regulates GPX4 [24]. In addition, GPX4 expression at gene level is also regulated by Sec-tRNA, which is one of the key regulatory elements during the maturation of GPX4 by incorporating selenium as a selenocysteine. At the translational level, the guanine-rich sequence-binding factor 1 has been reported to promote the translation of mitochondrial GPX4 during embryonic brain development [65]. Meanwhile, GPX4 protein level can also be regulated by posttranslational modification, as it has been uncovered to degrade *via* HSP90-mediated autophagy [66]. Ubiquitination and other degradation ways of GPX4 protein remains to be explored. In the case of GPX4 loss in ALS, the precise mechanism requires deep examination from transcriptional, translational and posttranslational modification perspectives.

Conclusion

This study characterizes the loss of GPX4, a key phospholipid peroxidation regulator, in the lumbar spines of ALS patients and mice. Moreover, PE(38:4) + 2O is identified as the main type of oxidized phospholipids in the spinal cord of ALS mice. Importantly, neuron-targeted *GPX4* gene therapy for scavenging phospholipids peroxidation in spinal cord is proposed as an essential therapeutic strategy to alleviate motor neuron loss, behavioral dysfunction, abnormal neuromuscular connection, and lumbar spine atrophy. Therefore, this study provides an important research basis for the application of GPX4 or other anti-peroxidation agents in anti-ALS treatments, albeit further studies on the molecular mechanisms of GPX4 in neuron degeneration and astrocyte activation are warranted.

Compliance with Ethics Requirements

All Institutional and National Guidelines for the care and use of animals (fisheries) were followed.

CRediT authorship contribution statement

Long-Fang Tu: Investigation, Data curation, Writing – original draft. **Tian-Ze Zhang:** Investigation. **Yang-Fan Zhou:** Validation. **Qing-Qing Zhou:** Validation. **Hai-Biao Gong:** Methodology. **Lei Liang:** Project administration, Funding acquisition. **Lin-Na Hai:** Validation. **Nan-Xin You:** Validation. **Yang Su:** Methodology. **Yong-Jun Chen:** Supervision. **Xu-Kai Mo:** Methodology. **Chang-Zheng Shi:** Supervision. **Liang-Ping Luo:** Supervision. **Wan-Yang Sun:** Formal analysis. **Wen-Jun Duan:** Visualization, Writing – review & editing, Funding acquisition. **Hiroshi Kurihara:** Supervision, Project administration. **Yi-Fang Li:** Writing – review & editing, Funding acquisition. **Rong-Rong He:** Conceptualization, Supervision, Funding acquisition.

Declaration of Competing Interest

The authors declare that they have no known competing financial interests or personal relationships that could have appeared to influence the work reported in this paper.

Acknowledgements

This work was supported, in part, by National Key Research and Development Program of China (2017YFC1700404), Natural Science Foundation of China (82125038, 81873209, U1801284, 81903821 and 81973718), the Local Innovative and Research Teams Project of Guangdong Pearl River Talents Program (2017BT01Y036), GDUPS (2019), Natural Science Foundation of Guangdong (2019A1515010909, 2021A1515011297), Science and Technology Program of Guangzhou (201903010062, 907158833068), and the Innovation Team Project of Guangdong Provincial Department of Education (2020KCXTD003). The authors (R.R. He and Y.F. Li) also gratefully acknowledge the support of K. C. Wong Education Foundation.

Appendix A. Supplementary material

Supplementary data to this article can be found online at https://doi.org/10.1016/j.jare.2022.02.016.

References

[1] Longo DL, Brown RH, Al-Chalabi A. Amyotrophic Lateral Sclerosis. N Engl J Med 2017;377(2):162–72.
[2] Kiernan MC, Vucic S, Cheah BC, Turner MR, Eisen A, Hardiman O, et al. Amyotrophic lateral sclerosis. Lancet 2011;377(9769):942–55.
[3] van Es MA, Hardiman O, Chio A, Al-Chalabi A, Pasterkamp RJ, Veldink JH, et al. Amyotrophic lateral sclerosis. Lancet 2017;390(10107):2084–98.
[4] Chiò A, Logroscino G, Hardiman O, Swingler R, Mitchell D, Beghi E, et al. Prognostic factors in ALS: A critical review. Amyotroph lateral Scler Off Publ World Fed Neurol Res Gr Mot Neuron Dis 2009;10(5-6):310–23.
[5] Nowicka N, Juranek J, Juranek JK, Wojtkiewicz J. Risk Factors and Emerging Therapies in Amyotrophic Lateral Sclerosis. Int J Mol Sci 2019 May;20 (11):2616. doi: https://doi.org/10.3390/ijms20112616.
[6] Xu Lu, Chen Lu, Wang S, Feng J, Liu L, Liu G, et al. Incidence and prevalence of amyotrophic lateral sclerosis in urban China: a national population-based study. J Neurol Neurosurg Psychiatry 2020;91(5):520–5.
[7] Arthur KC, Calvo A, Price TR, Geiger JT, Chiò A, Traynor BJ. Projected increase in amyotrophic lateral sclerosis from 2015 to 2040. Nat Commun 2016 Aug;7:12408.
[8] Le Gall L, Anakor E, Connolly O, Vijayakumar U, Duddy W, Duguez S. Molecular and Cellular Mechanisms Affected in ALS. J Pers Med 2020 Aug;10(3):101. doi: https://doi.org/10.3390/jpm10030101.
[9] Xiong L, McCoy M, Komuro H, West XZ, Yakubenko V, Gao D, et al. Inflammation-dependent oxidative stress metabolites as a hallmark of amyotrophic lateral sclerosis. Free Radic Biol Med 2022;178:125–33.
[10] Jackson C, Heiman-Patterson T, Kittrell P, Baranovsky T, McAnanama G, Bower L, et al. Radicava (edaravone) for amyotrophic lateral sclerosis: US experience at 1 year after launch. Amyotroph Lateral Scler Frontotemporal Degener 2019;20(7-8):605–10.
[11] Yoshino H. Edaravone for the treatment of amyotrophic lateral sclerosis. Expert Rev Neurother 2019;19(3):185–93.
[12] Chiò A, Mazzini L, Mora G. Disease-modifying therapies in amyotrophic lateral sclerosis. Neuropharmacology 2020;167:107986.
[13] Sultana R, Perluigi M, Butterfield DA. Lipid peroxidation triggers neurodegeneration: a redox proteomics view into the Alzheimer disease brain. Free Radic Biol Med 2013;62:157–69.
[14] Yang W, SriRamaratnam R, Welsch M, Shimada K, Skouta R, Viswanathan V, et al. Regulation of ferroptotic cancer cell death by GPX4. Cell 2014;156(1-2):317–31.
[15] Wang M, Liu C-Y, Wang T, Yu H-M, Ouyang S-H, Wu Y-P, et al. (+)-Clausenamide protects against drug-induced liver injury by inhibiting hepatocyte ferroptosis. Cell Death Dis 2020;11(9):781.
[16] Friedmann Angeli JP, Schneider M, Proneth B, Tyurina YY, Tyurin VA, Hammond VJ, et al. Inactivation of the ferroptosis regulator Gpx4 triggers acute renal failure in mice. Nat Cell Biol 2014;16(12):1180–91.
[17] Wang X, Michaelis EK. Selective neuronal vulnerability to oxidative stress in the brain. Front Aging Neurosci 2010;2:12.
[18] Simpson EP, Henry YK, Henkel JS, Smith RG, Appel SH. Increased lipid peroxidation in sera of ALS patients: a potential biomarker of disease burden. Neurology 2004;62(10):1758–65.
[19] Pisoschi AM, Pop A. The role of antioxidants in the chemistry of oxidative stress: A review. Eur J Med Chem 2015;97:55–74.
[20] Shibata N, Nagai R, Uchida K, Horiuchi S, Yamada S, Hirano A, et al. Morphological evidence for lipid peroxidation and protein glycoxidation in spinal cords from sporadic amyotrophic lateral sclerosis patients. Brain Res 2001;917(1):97–104.
[21] Smith RG, Henry YK, Mattson MP, Appel SH. Presence of 4-hydroxynonenal in cerebrospinal fluid of patients with sporadic amyotrophic lateral sclerosis. Ann Neurol 1998;44(4):696–9.
[22] Kagan VE, Mao G, Qu F, Angeli JPF, Doll S, Croix CS, et al. Oxidized arachidonic and adrenic PEs navigate cells to ferroptosis. Nat Chem Biol 2017;13(1):81–90.
[23] Jang S, Chapa-Dubocq XR, Tyurina YY, St Croix CM, Kapralov AA, Tyurin VA, et al. Elucidating the contribution of mitochondrial glutathione to ferroptosis in cardiomyocytes. Redox Biol 2021;45:102021.
[24] Savaskan NE, Ufer C, Kühn H, Borchert A. Molecular biology of glutathione peroxidase 4: from genomic structure to developmental expression and neural function. Biol Chem 2007 Oct;388(10):1007–17.
[25] Maiorino M, Conrad M, Ursini F. GPx4, Lipid Peroxidation, and Cell Death: Discoveries, Rediscoveries, and Open Issues. Antioxid Redox Signal 2018;29 (1):61–74.
[26] Yoo MH, Gu X, Xu XM, Kim JY, Carlson BA, Patterson AD, et al. Delineating the role of glutathione peroxidase 4 in protecting cells against lipid hydroperoxide damage and in Alzheimer's disease. Antioxid Redox Signal 2010;12(7):819–27.
[27] Bellinger FP, Bellinger MT, Seale LA, Takemoto AS, Raman AV, Miki T, et al. Glutathione Peroxidase 4 is associated with Neuromelanin in Substantia Nigra and Dystrophic Axons in Putamen of Parkinson's brain. Mol Neurodegener 2011;6(1):8.
[28] Li Q, Han X, Lan Xi, Gao Y, Wan J, Durham F, et al. Inhibition of neuronal ferroptosis protects hemorrhagic brain. JCI insight 2017;2(7):e90777.
[29] Chen L, Hambright WS, Na R, Ran Q. Ablation of the Ferroptosis Inhibitor Glutathione Peroxidase 4 in Neurons Results in Rapid Motor Neuron Degeneration and Paralysis. J Biol Chem 2015;290(47):28097–106.
[30] Schuster DJ, Dykstra JA, Riedl MS, Kitto KF, Belur LR, McIvor RS, et al. Biodistribution of adeno-associated virus serotype 9 (AAV9) vector after intrathecal and intravenous delivery in mouse. Front Neuroanat 2014;8:42.
[31] Hu H, Lin H, Duan W, Cui C, Li Z, Liu Y, et al. Intrathecal Injection of scAAV9-hIGF1 Prolongs the Survival of ALS Model Mice by Inhibiting the NF-kB Pathway. Neuroscience 2018;381:1–10.
[32] Zhang L, Haraguchi S, Koda T, Hashimoto K, Nakagawara A. Muscle atrophy and motor neuron degeneration in human NEDL1 transgenic mice. J Biomed Biotechnol 2011;2011:1–7.
[33] Deacon RMJ. Measuring the strength of mice. J Vis Exp 2013 Jun;76.
[34] Aartsma-Rus A, van Putten M. Assessing functional performance in the mdx mouse model. J Vis Exp 2014;85.
[35] Hatzipetros T, Kidd JD, Moreno AJ, Thompson K, Gill A, Vieira FG. A Quick Phenotypic Neurological Scoring System for Evaluating Disease Progression in the SOD1-G93A Mouse Model of ALS. J Vis Exp 2015 Oct;104.
[36] Folch J, Lees M, Stanley GHS. A simple method for the isolation and purification of total lipides from animal tissues. J Biol Chem 1957;226(1):497–509.
[37] Maniatis S, Äijö T, Vickovic S, Braine C, Kang K, Mollbrink A, et al. Spatiotemporal dynamics of molecular pathology in amyotrophic lateral sclerosis. Science 2019;364(6435):89–93.
[38] Golabchi FN, Sapienza S, Severini G, Reaston P, Tomecek F, Demarchi D, et al. Assessing aberrant muscle activity patterns via the analysis of surface EMG data collected during a functional evaluation. BMC Musculoskelet Disord 2019;20(1):13.
[39] Gatto RG, Li W, Magin RL. Diffusion tensor imaging identifies presymptomatic axonal degeneration in the spinal cord of ALS mice. Brain Res 2018;1679:45–52.
[40] Shaw B, Valentine J. How do ALS-associated mutations in superoxide dismutase 1 promote aggregation of the protein? Trends Biochem Sci 2007;32(2):78–85.
[41] Gurney ME. The use of transgenic mouse models of amyotrophic lateral sclerosis in preclinical drug studies. J Neurol Sci 1997 Oct;152(Suppl 1): S67–73.
[42] Stockwell BR, Friedmann Angeli JP, Bayir H, Bush AI, Conrad M, Dixon SJ, et al. Ferroptosis: A Regulated Cell Death Nexus Linking Metabolism, Redox Biology, and Disease. Cell 2017;171(2):273–85.
[43] Brigelius-Flohé R, Maiorino M. Glutathione peroxidases. Biochim Biophys Acta 2013;1830(5):3289–303.
[44] Ribas V, García-Ruiz C, Fernández-Checa JC. Glutathione and mitochondria. Front Pharmacol 2014;5:151.
[45] Hirrlinger J, Dringen R. The cytosolic redox state of astrocytes: Maintenance, regulation and functional implications for metabolite trafficking. Brain Res Rev 2010;63(1-2):177–88.
[46] Díaz-Amarilla P, Olivera-Bravo S, Trias E, Cragnolini A, Martínez-Palma L, Cassina P, et al. Phenotypically aberrant astrocytes that promote motoneuron damage in a model of inherited amyotrophic lateral sclerosis. Proc Natl Acad Sci USA 2011;108(44):18126–31.
[47] Turner MR, Hardiman O, Benatar M, Brooks BR, Chio A, de Carvalho M, et al. Controversies and priorities in amyotrophic lateral sclerosis. Lancet Neurol 2013;12(3):310–22.
[48] Oskarsson B, Gendron TF, Staff NP. Amyotrophic Lateral Sclerosis: An Update for 2018. Mayo Clin Proc 2018;93(11):1617–28.
[49] Patel D, Witt SN. Ethanolamine and Phosphatidylethanolamine: Partners in Health and Disease. Oxid Med Cell Longev 2017;2017:1–18.
[50] Calzada E, Onguka O, Claypool SM. Phosphatidylethanolamine Metabolism in Health and Disease. Int Rev Cell Mol Biol 2016;321:29–88.
[51] Gautam M, Jara JH, Kocak N, Rylaarsdam LE, Kim KD, Bigio EH, et al. Mitochondria, ER, and nuclear membrane defects reveal early mechanisms for upper motor neuron vulnerability with respect to TDP-43 pathology. Acta Neuropathol 2019;137(1):47–69.
[52] Yang WS, Stockwell BR. Ferroptosis: Death by Lipid Peroxidation. Trends Cell Biol 2016;26(3):165–76.
[53] Yang WS, Kim KJ, Gaschler MM, Patel M, Shchepinov MS, Stockwell BR. Peroxidation of polyunsaturated fatty acids by lipoxygenases drives ferroptosis. Proc Natl Acad Sci USA 2016;113(34):E4966–75.
[54] Meyer K, Ferraiuolo L, Miranda CJ, Likhite S, McElroy S, Renusch S, et al. Direct conversion of patient fibroblasts demonstrates non-cell autonomous toxicity of astrocytes to motor neurons in familial and sporadic ALS. Proc Natl Acad Sci USA 2014;111(2):829–32.
[55] Puentes F, Malaspina A, van Noort JM, Amor S. Non-neuronal Cells in ALS: Role of Glial, Immune cells and Blood-CNS Barriers. Brain Pathol 2016;26 (2):248–57.
[56] Liddelow SA, Guttenplan KA, Clarke LE, Bennett FC, Bohlen CJ, Schirmer L, et al. Neurotoxic reactive astrocytes are induced by activated microglia. Nature 2017;541(7638):481–7.
[57] Luo X, Gong H-B, Gao H-Y, Wu Y-P, Sun W-Y, Li Z-Q, et al. Oxygenated phosphatidylethanolamine navigates phagocytosis of ferroptotic cells by interacting with TLR2. Cell Death Differ 2021;28(6):1971–89.
[58] Ioannou MS, Jackson J, Sheu S-H, Chang C-L, Weigel AV, Liu H, et al. Neuron-Astrocyte Metabolic Coupling Protects against Activity-Induced Fatty Acid Toxicity. Cell 2019;177(6):1522–1535.e14.
[59] Ma W, Zhan Y, Zhang Y, Xie X, Mao C, Lin Y. Enhanced Neural Regeneration with a Concomitant Treatment of Framework Nucleic Acid and Stem Cells in Spinal Cord Injury. ACS Appl Mater Interfaces 2020;12(2):2095–106.

[60] Zhang T, Tian T, Lin Y. Functionalizing Framework Nucleic Acid-Based Nanostructures for Biomedical Application. Adv Mater 2021 Nov;17(2): e2107820.
[61] Sneddon AA, Wu H-C, Farquharson A, Grant I, Arthur JR, Rotondo D, et al. Regulation of selenoprotein GPx4 expression and activity in human endothelial cells by fatty acids, cytokines and antioxidants. Atherosclerosis 2003;171(1):57–65.
[62] Ursini F, Maiorino M. Lipid peroxidation and ferroptosis: The role of GSH and GPx4. Free Radic Biol Med 2020;152:175–85.
[63] Alim I, Caulfield JT, Chen Y, Swarup V, Geschwind DH, Ivanova E, et al. Selenium Drives a Transcriptional Adaptive Program to Block Ferroptosis and Treat Stroke. Cell 2019;177(5):1262–1279.e25.
[64] Tang D, Chen X, Kang R, Kroemer G. Ferroptosis: molecular mechanisms and health implications. Cell Res 2021;31(2):107–25.
[65] Ufer C, Wang CC, Fähling M, Schiebel H, Thiele BJ, Billett EE, et al. Translational regulation of glutathione peroxidase 4 expression through guanine-rich sequence-binding factor 1 is essential for embryonic brain development. Genes Dev 2008;22(13):1838–50.
[66] Wu Z, Geng Y, Lu X, Shi Y, Wu G, Zhang M, et al. Chaperone-mediated autophagy is involved in the execution of ferroptosis. Proc Natl Acad Sci USA 2019;116(8):2996–3005.